

Modeling seasonal salinity variations in a large West African lagoon (Nokoué, Benin): major drivers and mechanisms

Okpeitcha Olaègbè Victor ^{1,2,3,*}, Chaigneau Alexis ^{2,3,4}, Morel Yves ^{4,5}, Duhaut Thomas ⁴, Marsaleix Patrick ⁴, Rétif Fabien ⁶, Honfo Jules ^{2,4}, Stieglitz Thomas ⁷, Sohou Zacharie ^{3,8}, Sintondji Luc Olivier ¹, Mama Daouda ¹

¹ Laboratoire d'Hydrologie Appliquée (LHA), Institut National de l'Eau (INE), African Centre of Excellence for Water and Sanitation (C2EA), Université d'Abomey Calavi, Bénin

² International Chair in Mathematical Physics and Applications (ICMPA–UNESCO Chair)/University of Abomey-Calavi, Cotonou, Benin

³ Institut de Recherches Halieutiques et Océanologiques du Bénin (IRHOB), Cotonou, Benin

⁴ Laboratoire d'Études en Géophysique et Océanographie Spatiale (LEGOS), Université de Toulouse, CNES, CNRS, IRD, UPS, Toulouse, France

⁵ Laboratoire d'Océanographie Physique et Spatiale (LOPS), University of Brest, CNRS, IRD, Ifremer, IUEM, France

⁶ SNALE, Aubenas, France

⁷ Aix-Marseille Université, CNRS, IRD, INRAE, CEREGE, Aix-en-Provence, France

⁸ Département de Zoologie, Faculté des Sciences et Techniques (FAST/UAC), Bénin

* Corresponding author : Olaègbè Victor Okpeitcha, email address : vokpeitcha@gmail.com

Abstract :

Nokoué lagoon is a shallow water body connected to the Gulf of Guinea through the long and narrow Cotonou channel. The salinity dynamics in the lagoon is investigated using the 3D SYMPHONIE numerical model. We first validate the model using salinity and water level data. Simulated and observed salinity and water level variations compare well demonstrating that the reference model simulation correctly reproduces the dynamics of the lagoon. By performing several simulations with varying external forcings and freshwater fluxes, the main drivers of salinity variability in the lagoon are identified.

We first focus on the salinization phase of the lagoon at the end of the tropical wet season (between November and February), and we investigate the total change in salinity and the salt fluxes involved in these variations. The high frequency salt fluxes associated with the ocean tide import salt from the ocean via the Cotonou channel to the south of the lagoon. Baroclinic fluxes, associated with the influence of salt on density and associated pressure gradient, increase this local salinity input in the south, but also play a major role in the dispersion of salt throughout the lagoon. Two rivers provide a permanent freshwater inflow in the north/ northeast of the lagoon that limits the salinization of the whole lagoon. Finally, wind-generated high frequency recirculation, partially prevents the salinisation of the North-East of the lagoon.

During the desalinization period (between May and September), the lagoon salinity variations are highly sensitive to the magnitude of river inflow. At a constant river flux rate, the lagoon attains an equilibrium state in salinity. As this equilibrium is reached, both the overall salinity level and the time needed to

achieve it decrease notably with higher fluxes. Beyond 100 m³ s⁻¹, only a small area near the Cotonou channel retains higher salinity, while surpassing 500 m³ s⁻¹ results in complete desalination of the entire Nokoué lagoon.

Highlights

► The Nokoué Lagoon's dynamics is accurately captured by the 3D SYMPHONIE model. ► High-frequency salt fluxes related to tides import salt to the South of the Lagoon. ► Baroclinic fluxes greatly contribute to the dispersion of salt across the Lagoon. ► Winds mitigate the salinization process in the North-Eastern part of the Lagoon. ► Nokoué Lagoon is highly sensitive to river discharge, especially during low flow.

Keywords : Lagoon, Salinity variability, numerical model, physical processes.

1. Introduction

Coastal lagoons are highly valuable components of the natural heritage and ecosystems in the coastal zone providing important ecosystem services such as agricultural, tourism and fisheries development (Gonenc & Wolflin, 2004). They are highly variable and productive environments (Kjerfve, 1994), and occupy ~13% of the world's coastal zone, including 18% of the African coast (Cromwell, 1971; Barnes, 1980). Coastal lagoons are the dominant features along the West African coast (Pauly, 1975) and cover an area of ~ 3,000 km² between Ivory Coast and Nigeria (A. P. Lalèyè et al., 2007).

Nokoué Lagoon is one of the most important lagoons along the West African coast in terms of biological productivity, ecological and economic values (Djihouessi et al., 2017; A. P. Lalèyè et al., 2007). It is exploited by ~ 12,000 fishermen (Latifou et al., 2020) and contributes to nearly 65% of Benin's continental fishery catches. Nokoué lagoon also hosts the largest lacustrine villages in West Africa (Djihouessi & Aina, 2018; Yehouenou et al., 2013) and more than one million people live in the immediate vicinity of the lagoon (Gnohossou, 2006). Nokoué lagoon and the surrounding wetlands host a large biodiversity and are classified as protected areas by the Ramsar agreement (<https://rsis.ramsar.org/fr/ris/1018>). Overall, the lagoon environment

presents very important socio-economic benefits for the development of Benin, and it is important to better understand its functioning to ensure its preservation.

Salinity is one of the key factors affecting coastal lagoon ecosystems (Attrill, 2002; García-Oliva et al., 2019; Nunes et al., 2021), controlling the diversity and abundance of fish, the distribution of plankton and the biomass of aquatic plants (Dube et al., 2010; Franco et al., 2019; Nunes et al., 2021). Salinity depends on ocean and river inputs into the lagoon and is very sensitive to physical drivers influencing the hydrodynamics of the lagoon, such as tide, wind (Alekseenko et al., 2017; Cerralbo et al., 2016; Mahanty et al., 2016) or the baroclinic pressure gradient, due to density difference between saline and freshwater (e.g. Gross et al., 1999).

The Nokoué Lagoon is primarily fed by substantial freshwater inputs from the Sô and Ouémé rivers in its northern region, along with a minor contribution from the smaller Djonou river in the southwest (Fig. 1). It maintains a continuous exchange of saltwater with the Atlantic Ocean through the Cotonou channel (Fig. 1), primarily influenced by ocean tides (Okpeitcha et al. in 2022). Seasonal variations of freshwater discharge into Nokoué lagoon increase its water level by ~1 m between the dry and wet (African Monsoon) seasons (Chaigneau et al., 2022; Morel et al., 2022), and the mean lagoon salinity increases from 0 in flood period to 25 in the lowest water period (Okpeitcha et al., 2022). These variations in salinity are crucial for the composition and structuring of the Nokoué lagoon ecosystems, from plankton to fish (Chaigneau et al., 2023; P. Lalèyè et al., 2003; Odountan et al., 2019).

Generally, seasonal variations of lagoon salinity are first order driven by the tide and river discharges. This is also documented for Nokoué lagoon (Djihouessi & Aina, 2018; Laleye, 1995; Le Barbé et al., 1993; Okpeitcha et al., 2022; Zandagba et al., 2016). In a recent study, based on in-situ observations and a simplified box model,

Okpeitcha et al. (2022) showed the high sensitivity of the lagoon's salinity to flow variations and estimated that the lagoon could be fully desalinated for a river flow rate greater than $\sim 50\text{-}60 \text{ m}^3 \text{ s}^{-1}$. In addition, they estimated that baroclinic effects related to the salinity and pressure gradients may cause an additional average transport of approximately $40 \text{ m}^3 \text{ s}^{-1}$ of ocean water into the lagoon, in conjunction with the advective exchange driven by tides.

In this study, we analyse the salinity variability in the Nokoué lagoon using a realistic 3D numerical model. We first describe the numerical configuration and the in-situ data available for the model validation (Section 2). The methodology, based on a temporal coarse grain analysis of salt fluxes, is also presented (Section 2.4). The reference simulation is presented and validated in Section 3.1. We then evaluate the influence of key driving processes: tide, salt gradient, wind, river discharge (Section 3.2). Finally, we investigate the role of freshwater fluxes and determine the threshold over which ocean waters and salt cannot penetrate the lagoon.

2. Study area, model and datasets

2.1. Study area

The Nokoué lagoon is a choked coastal lagoon spanning approximately 20 km from West to East and 11 km from South to North (Gadel & Texier, 1986; Le Barbé et al., 1993). This shallow lagoon has a mean depth of 1.3 m and 2.2 m during low and high-water seasons, respectively (Chaigneau et al., 2022). It is the largest brackish water body of Benin, covering an area $\sim 150\text{-}170 \text{ km}^2$ during dry and wet seasons and with a volume of $1.5 \times 10^8 \text{ m}^3$ during low water periods (Le Barbé et al., 1993). The lagoon is connected to the Atlantic Ocean via the Cotonou channel, which is approximately 4.5

km long and 400 m wide (Fig. 1c). The amplitude of semi-diurnal tide is strongly attenuated within the lagoon compared to the ocean, with 55-90 cm in the ocean to about 3-5 cm within the lagoon (Chaigneau et al., 2022).

Nokoué lagoon receives freshwater from multiple sources, the main ones are the Sô and Ouémé rivers in the northern part of the lagoon (Fig. 1c), which have catchment areas of 50,000 km² and 1,000 km², respectively (Djihouessi & Aina, 2018; Le Barbé et al., 1993). In addition, small amounts of fresh water enter the lagoon from e.g. the Djonou river located southwest of the area and Totchè channel (Le Barbé, 1993; Texier et al., 1980; Djihouessi & Aina, 2018). The seasonal cycle of the regional climate is dominated by the West African monsoon (Fink et al., 2017) with two dry and two rainy seasons (Ahokpossi, 2018; N'Tcha M'Po et al., 2017; Guedje et al., 2019). The long dry season lasts from December to February, while the short one is from August to September (Guedje et al., 2019). The main rainy season occurs from March to July, with a peak in June, while the short rainy season runs from September to November (Ahokpossi, 2018; N'Tcha M'Po et al., 2017). The annual average rainfall is ~1300 mm (Biao, 2017; Lawin et al., 2019; Mama, 2010). However, it is important to note that these double rainy seasons have no significant effect on Nokoué lagoon water level (Chaigneau et al., 2022). Instead, the water level is significantly influenced by the discharge of water from the Ouémé and Sô catchments from the northern part of Benin. In this region to the north of the lagoon, a single rainy season lasts from April to October with the highest rainfall occurring in August (Ahokpossi, 2018; Biao, 2017; Lawin et al., 2019; N'Tcha M'Po et al., 2017). During this period, the lagoon water level increases by ~1 m (Chaigneau et al., 2022) and its salinity reduces to zero (Djihouessi & Aina, 2018; Okpeitcha et al., 2022). Thus, the hydrological regime of the lagoon is primarily influenced by the seasonal variations of river discharges. Unfortunately, there

are no direct measurements of river discharges into Nokoué lagoon, and estimates of peak fluxes during the rainy season vary widely, ranging from $\sim 400 \text{ m}^3 \text{ s}^{-1}$ to $\sim 1,000 \text{ m}^3 \text{ s}^{-1}$ (Djihouessi et al., 2019; Lawin et al., 2019; Le Barbé et al., 1993). However, a recent study by Morel et al. (2022) proposed a method to estimate the net fluxes to the lagoon using observations of water level variations and tide amplitude. Applying this method to data acquired in 2018, they confirmed a maximum net flux of $\sim 1,100 \text{ m}^3 \text{ s}^{-1}$.

The prevailing winds in the study area are characterized by southwesterly winds from the ocean throughout the year, except during the long dry season when northeasterly winds called Harmattan can episodically occur from December to March (Bajamgnigni Gbambie & Steyn, 2013; Guedje et al., 2019). The monthly average wind speed varies between 2 and 5 $\text{m}\cdot\text{s}^{-1}$ with a main peak in August and a secondary one in March (Guedje et al., 2019).

2.2. SYMPHONIE model

2.2.1. Model description

Numerical simulations were carried out using SYMPHONIE model (Marsaleix et al., 2008), a three-dimensional (3D) free surface hydrodynamical model, solving the Navier-Stokes equations using the Boussinesq and hydrostatic approximations. The free surface variations at high frequency (mostly associated with surface gravity waves) are taken into account using a time splitting method (Marsaleix et al., 2008). The state variables (current, temperature, salinity, surface elevation) are calculated on an Arakawa C-grid (Arakawa & Lamb, 1977) and a generalised sigma vertical coordinates (terrain following coordinate), using an energy-conserving finite difference method (Marsaleix et al., 2008, 2012, 2019). We have chosen a free slip bottom

boundary condition, for which the terrain following coordinate ensures a perfect representation. This is of particular importance for such a shallow lagoon, since spurious effects at the bottom (such as staircase representation for z Cartesian coordinate) can strongly influence the dynamics over the whole water column. The turbulence variables (turbulent vertical mixing coefficients, turbulent kinetic energy and its dissipation rate) are calculated by the K-epsilon scheme as in Costa et al., (2017).

2.2.2. Model set up

For our study, the configuration used extends between longitudes 2.26°E and 2.76°E and between latitudes 6.11°N and 6.55°N (Fig. 1) with 563×646 horizontal grid points. To correctly represent the dynamics in the Cotonou Channel and the lagoon, a curvilinear bipolar grid is used with horizontal resolution varying from ~ 40 m in the Cotonou Channel to ~ 250 m at the open ocean boundary (Fig. 1c). To correctly resolve the hydrodynamic conditions of this shallow lagoon, 10 vertical levels were used. The bathymetry used merges over 123,000 depth soundings in the lagoon and rivers (Chaigneau et al., 2022) complemented by GEBCO (GEBCO_08 Grid, version 20090202, <http://www.gebco.net>) in the coastal ocean.

The model is forced by large-scale ocean conditions, ocean tide, freshwater inflow from rivers, wind, and atmospheric conditions.

Oceanic forcing (temperature, salinity, Sea Surface Height, currents) at the open-ocean boundary (Marsaleix et al., 2006) are based on daily outputs from the MERCATOR-Ocean (Lellouche et al., 2013) global configuration at $1/12^{\circ}$ spatial resolution (version PSY4QV3R1).

Tidal forcing is performed at the ocean boundary using the FES2014 solution (Carrere et al., 2016), and 9 (M_2 , N_2 , S_2 , K_2 , K_1 , O_1 , P_1 , Q_1 , M_4) main tidal harmonic constituents are used.

Meteorological forcing fields were obtained from ECMWF three-hourly and $1/8^\circ$ spatial resolution forecasts (wind speed at 10m, temperature and specific humidity at 2m, surface pressure, precipitation, solar fluxes and thermal radiative fluxes) using COARE bulk formulae (Fairall et al., 2003).

River discharges entering the lagoon during flood periods were estimated by Morel et al. (2022). Fluxes during low water periods are more difficult to estimate and required calibration. To account for this, we conducted sensitivity analyses and determined that a minimum flux of $7.5 \text{ m}^3 \text{ s}^{-1}$ was necessary to realistically simulate lagoon desalination near the rivers.

Three freshwater inputs were considered: the Djonou River, the Sô River and the Ouémé River (Fig. 1). The net river discharge into the lagoon varied from $\sim 7.5 \text{ m}^3 \text{ s}^{-1}$ in the dry season to a maximum of $\sim 1100 \text{ m}^3 \text{ s}^{-1}$ during the wet season (Chaigneau et al., 2022; Morel et al., 2022). Historical data from the SIEREM database (<http://www.hydrosciences.org/spip.php?article1236>) indicated that the Ouémé and Sô rivers contributed approximately to 70% and 30%, respectively, of the total river discharge feeding into the lagoon from the northern side. Although the Djonou river lacked measurement gauges, recent estimations suggest that this smaller river might contribute approximately 2% to the overall flow entering the lagoon. Without any complementary information or observations, we assumed these percentages remained correct.

Our simulations cover the period between October 2016 and December 2018, with a 12-month spin-up period from October 2016 to September 2017. Therefore, the retained simulation extended from October 2017, when the lagoon was devoid of salt, to December 2018. A computational time step of $\sim 30 \text{ s}$ was determined to satisfy the CFL condition (Blumberg & Mellor, 1987; Marsaleix et al., 2012) for our simulations.

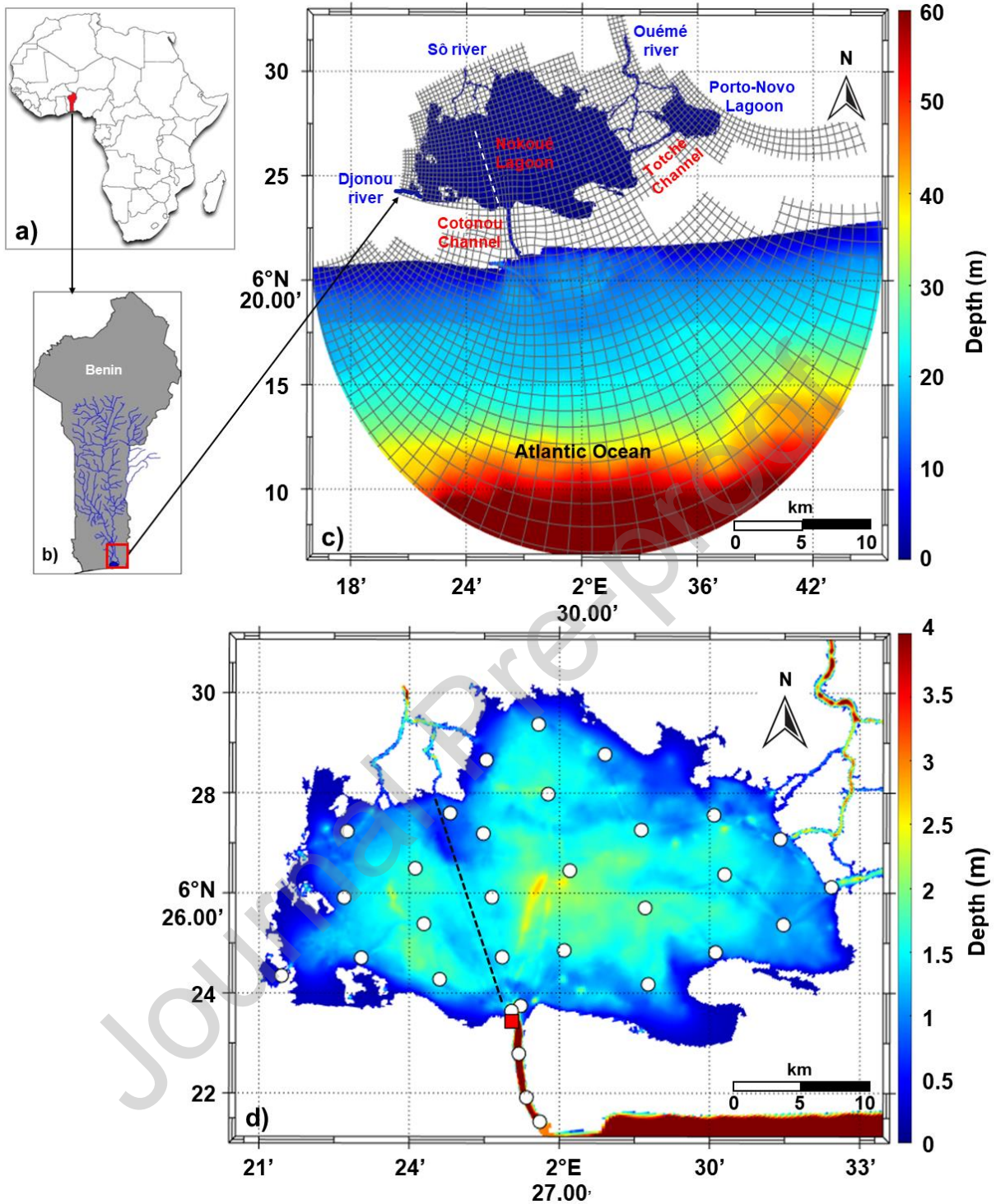


Fig. 1. Study area in southern Benin (West Africa), showing (a) the location of Benin, (b) the hydrographic network of the Sô and Ouémé catchments in Benin, (c) the SYMPHONIE model grid (each cell representing 10 grid points) and bathymetry of model domain, d) bathymetry of the Nokoué lagoon. The 31 CTD observation stations performed monthly between December 2017 and December 2018 are marked by white dots in d), the water level data logger position is shown by a red square, and the black dashed line represents the location of south-north high CTD resolution section.

2.2.3. Numerical simulations

In this study, we construct a reference simulation (*Ref*) as the most realistic representation of the Nokoué Lagoon's salinity dynamics, which considers the physical drivers and calibrations previously described. To understand the importance of each driver, we conducted three additional simulations:

- *NoTide*, in which the tidal forcing was removed while keeping all other forcings as in the reference simulation.

- *NoSal*, in which the effect of salt in the density equation of state was removed within the lagoon, to isolate the baroclinic effects associated with salinity gradients between the ocean and the lagoon. However, the pressure gradient effects of salt were retained in the ocean, maintaining the equation of state's integrity. Along the Cotonou channel, which connects the two zones, a linear adjustment was implemented to smoothly transition between the two regimes, accommodating both the inclusion and exclusion of salt in the equation of state. This simulation was designed to discern the specific impact of baroclinic effects within the Nokoué Lagoon, a factor estimated previously using a rudimentary box model to account for an average transport of approximately $40 \text{ m}^3 \text{ s}^{-1}$ (Okpeitcha et al., 2022). By isolating these effects, the *NoSal* scenario provides valuable insights into the role of salinity gradients and baroclinic effects in shaping lagoon dynamics and salinity fluxes.

- *NoWind*, in which the wind stress was removed from the momentum forcing but kept in the mixing closure scheme.

These 3 simulations were conducted from October 2017 to December 2018 and were used to investigate the impact of each forcing on the salinization phase of the lagoon observed between November 2017 and February 2018. To further study the sensitivity of the lagoon's salinity to variations in river inflow, we conducted 13 additional

simulations during the desalinization phase (May to September 2018). These *RunOffs* simulations involved the addition of constant river discharge increments, ranging from $30 \text{ m}^3 \text{ s}^{-1}$ to $900 \text{ m}^3 \text{ s}^{-1}$, to the dry season outflow of the *Ref* configuration ($\sim 7.5 \text{ m}^3 \text{ s}^{-1}$), starting from May 1, 2018 (beginning of the desalinization phase). The distribution of flux rates between the Djonou, the Sô and the Ouémé rivers was kept constant across all simulations. A description of each simulation is provided in Table 1.

Table 1. Summary of Reference and sensitivity simulations

Numerical simulation	Tidal Forcing	Wind Forcing	Baroclinic Forcing	River Forcing	Other Forcings
<i>Ref</i>	Yes	Yes	Yes	Yes	Yes
<i>NoTide</i>	No	Yes	Yes	Yes	Yes
<i>NoSal</i>	Yes	Yes	No	Yes	Yes
<i>NoWind</i>	Yes	No	Yes	Yes	Yes
<i>RunOffs</i>	Yes	Yes	Yes	Constant value	Yes

2.3. In-situ data

In order to evaluate the model results, we used measured salinity and water-level data. Salinity data were collected during 13 monthly surveys between December 2017 and December 2018, with each survey including approximately 31 vertical temperature and salinity profiles taken over Nokoué Lagoon using a Conductivity Temperature Depth (CTD) probe (Valeport MIDAS CTD+ 300, white dots in Fig. 1c). The CTD was sampled at a rate of 8 Hz and parameters were recorded every $\sim 10 \text{ cm}$

from the surface to the bottom. Only the descent CTD profiles were used. An objective interpolation method (Bretherton et al., 1976; McIntosh, 1990; Wong et al., 2003) was used to spatially interpolate the 31 irregularly distributed salinity data onto a regular grid of $\sim 100 \text{ m} \times 100 \text{ m}$ resolution. Additionally, high spatial resolution CTD data were collected over a south-north section during each survey, consisting of 24 stations spaced 250 m apart, from the Cotonou channel entrance to the mouth of the Sô river (white dashed line in Fig. 1c). Further information regarding the salinity dataset can be found in Okpeitcha et al. (2022).

Water-level measurements were acquired by a submerged pressure sensor (HOBO U20L-01, (Abimbola et al., 2020; Guragai et al., 2018) installed in the southwestern part of the lagoon, where it connects with the Cotonou channel (red square in Fig. 1c). This sensor recorded the absolute water pressure every 20 minutes since February 2018, providing a continuous measurement of water level variations in the lagoon. The water level data are considered representative of the overall water level changes in the lagoon; a detailed analysis of the dataset is available in Chaigneau et al. (2022).

2.4. Mean salt flux decomposition

In the following section, the model results will be analysed to study the mechanisms that are responsible for the salt variations in the lagoon during the salinization phase. In the model, the equation for the evolution of salinity is a simple advection diffusion equation and can be written in terms of fluxes

$$\partial_t S = -\text{div}(\vec{U}S) + \partial_z(K_z \partial_z S)$$

where S is salinity, \vec{U} the 3D velocity field and K_z the diffusion coefficient. Integrating over a time period $[0, T]$ the net variation of salinity can be related to mean fluxes over the time period, as:

$$S(T) - S(t = 0) = -\text{div}(\overline{\vec{U}S}) + \partial_z(\overline{K_z \partial_z S}).$$

We concentrate on the contribution of horizontal salt fluxes at different timescales. The mean horizontal salt flux US over a period $\Delta T < T$ (denoted $\overline{US}^{\Delta T}$) is decomposed into an average term and a fluctuation term:

$$\overline{US}^{\Delta T} = \overline{U}^{\Delta T} \overline{S}^{\Delta T} + \overline{U'S'}^{\Delta T} \quad (1)$$

where $\overline{U}^{\Delta T}$ et $\overline{S}^{\Delta T}$ represent the average values of velocity and salinity respectively over a period ΔT , U' et S' are the fluctuations around the mean. Thus, the term

$$\overline{U'S'}^{\Delta T} = \overline{US}^{\Delta T} - \overline{U}^{\Delta T} \overline{S}^{\Delta T} \quad (2)$$

represents the effect of processes with periods less than ΔT , on the total fluxes during ΔT .

Now, over $[0, T]$, the total salt flux can be obtained by integrating (1):

$$\overline{US}^T = \overline{U}^{\Delta T} \overline{S}^{\Delta T} + \overline{U'S'}^{\Delta T} \quad (3)$$

which leads to

$$\overline{U'S'}^{\Delta T} = \overline{US}^T - \overline{U}^{\Delta T} \overline{S}^{\Delta T} \quad (4)$$

$\overline{U'S'}^{\Delta T}$ here represents the net effect of processes with period less than ΔT on the total salt fluxes over the whole period $[0, T]$.

By distinguishing two periods $\Delta T_1 < \Delta T_2$, we deduce from equation (4) that:

$$\overline{U'S'}^{[\Delta T_1, \Delta T_2]} = \overline{US}^{\Delta T_2} - \overline{U'S'}^{\Delta T_1} = \overline{U}^{\Delta T_1} \overline{S}^{\Delta T_1} - \overline{U}^{\Delta T_2} \overline{S}^{\Delta T_2} \quad (5)$$

where $\overline{U'S'}^{[\Delta T_1, \Delta T_2]^T}$ represents the net effect of processes associated with time periods between $[\Delta T_1, \Delta T_2]$ on the total salt fluxes over the period $[0, T]$.

This approach is similar to the method of coarse grain decomposition (see Aluie et al., 2018, and references therein) but applied to time instead of space.

In our study, we first select a global time period T , which corresponds to the salinization period from mid-November to mid-February (see Section 3.2 and Okpeitcha et al., 2022). From equation (5), we then decomposed the total salt flux over this salinization period into a sum of fluxes over sub-periods smaller than T . While the semi-diurnal tide dominates, the O1 and K1 component, and other forcings -such as wind- are associated with significant diurnal variability (see Chaigneau et al., 2022). The basic period retained in this study is thus twice the semi-diurnal lunar period, related to all high frequency processes, $[0, T_{HF} = 24h50]$. We then consider the periods which is specific to spring/neap tides $[T_{HF}, T_{15d} = 14 T_{HF}]$ and the low frequency $[14 T_{HF}, T]$.

Thus, the contributions of these different temporal sub-periods to the total flux over the salinization period can be written respectively:

$$\overline{U'S'}^{[0, T_{HF}]^T} = \overline{US}^T - \overline{U}^{T_{HF}} \overline{S}^{T_{HF}} \quad (6)$$

$$\overline{U'S'}^{[T_{HF}, T_{15d}]^T} = \overline{U}^{T_{HF}} \overline{S}^{T_{HF}} - \overline{U}^{T_{15d}} \overline{S}^{T_{15d}} \quad (7)$$

$$\overline{U'S'}^{[T_{15d}, T]^T} = \overline{U}^{T_{15d}} \overline{S}^{T_{15d}} - \overline{U}^T \overline{S}^T \quad (8)$$

By combining the different terms of equations (6), (7) and (8) member by member, we obtain:

$$\overline{US}^T = \overline{U}^T \overline{S}^T + \sum_n \overline{U'S'}^{[T_n, T_{n+1}]^T} \quad (9)$$

with n the number of sub-periods (3 in our case). Note that each term in equations (6-9) can be calculated from the fields $\overline{US}^{T_{HF}}$, $\overline{U}^{T_{HF}}$ and $\overline{S}^{T_{HF}}$, which are stored during the simulation.

3. Results and discussion

3.1. Model validation

3.1.1. Salinity distribution

Figure 2 presents a comparison between the modeled monthly salinity distribution and the observed values, taken both at the surface and bottom of the lagoon. In situ salinity data were collected on a monthly basis within a relatively short time period of 2 days. Consequently, to validate the model, the salinity outputs were averaged over the 2-day duration of each field campaign. It is worth noting that conducting a more precise extraction of the model's salinity fields at the closest time of each CTD measurement did not yield any significant deviations in the results.

The salinization of the lagoon starts at the bottom layer in the southwest during December (Dec-2017 and Dec-2018), at the beginning of the dry season (Fig. 2b). From January to April, salinity gradually increases, with the lagoon bottom always saltier than the surface (Fig. 2a and b). The maximum salinity observed in April reaches up to 35 in the South of the lagoon and 25 in the North near the river mouths. From May to August, during the main wet season in southern Benin, salinity decreases rapidly, with the western part of the lagoon being saltier than the eastern part. The difference in salinity between the West and East in August is ~ 4 . During the flood period (September-November), which is the second wet season, the entire lagoon is filled with fresh water, and no salt is observed in either the model or the observations.

The model realistically reproduces the spatial and seasonal distributions of the observed salinity. In particular, it reproduces the gradual increase in salinity observed between December and April, both at the surface and at the bottom, as well as the important differences between surface and bottom, indicating marked vertical stratification, especially in December-January (see also Section 3.1.2). The model also captures the desalinisation phase observed between May and August at the end of the main wet season. The spatial salinity patterns observed in the lagoon, including the gradient from the Cotonou channel towards the North, where the lowest salinity values are observed at the river mouths, are qualitatively reproduced by the model. However, it should be noted that the model shows slight discrepancies in salinity levels compared to the observations. Specifically, the model shows lower salinity than observed in December and slightly higher salinity in May. These disparities could be linked to the model's empirical estimation of river fluxes, detailed in Section 2.2.2. Variations in both climatological data driving the model's river discharge and the actual 2017-2018 river discharge, as well as differences in distribution among contributing rivers (Sô, Ouémé, Djonou), contribute to discrepancies between observed and modeled salinity, particularly noticeable during salinization and desalination phases.

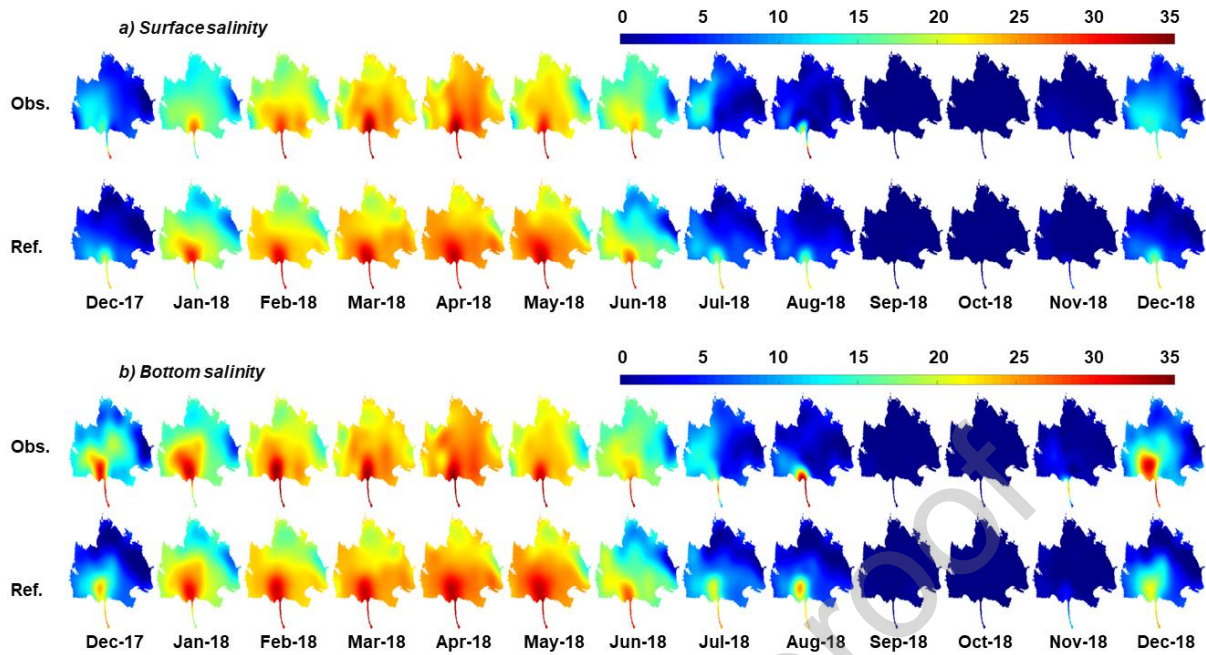


Fig. 2. Comparison of monthly (a) surface and (b) bottom salinity in the Nokoué lagoon between December 2017 and December 2018, as observed (top row) and modelled (bottom row).

Figures 3a and 3c demonstrate the strong agreement between the modelled salinity fields, extracted at the CTD measurement locations, and the corresponding in-situ data, both at the surface (Fig. 3a) and the bottom (Fig. 3c). Notably, a nearly linear relationship is observed between the modelled and observed data, with a global correlation coefficient of 0.94 at the surface and 0.93 at the bottom. The lowest correlation coefficients are found during the desalination phase, with values of 0.3 (0.6, respectively) at the surface (bottom) in July (represented by blue dots in Fig. 3a and 3c), and 0.8 (0.7) at the surface (bottom) in August (represented by black dots in Fig. 3a and 3c). Notably, discrepancies observed during the transitional phases of salinization/desalinization, especially in regions of relatively low salinity near the river mouths, may be linked to subtle differences between the mean seasonal cycle of river discharge used to drive the model and the actual 2017-2018 river discharge. Slight

variations in the volume and timing of river discharge between the datasets are likely contributing to localized discrepancies in salinity.

Figures 3b and d display the monthly average surface and bottom salinities across the entire Nokoué lagoon, with each monthly value representing a 2-day average. As shown, these salinities exhibit large seasonal variations. Specifically, from December to April, both surface and bottom salinities experience a rapid increase, peaking at 25 in April. Subsequently, from May to August, salinity decreases, reaching a minimum of 5 at both the surface and bottom. From September to November, the lagoon becomes filled with freshwater, rendering salinity negligible.

The model performs well in capturing the observed global average salinity variations for both the surface (Fig. 3b) and bottom (Fig. 3d) of the lagoon. However, some discrepancies are evident. In December (at the onset of salinization), the model tends to underestimate the observations, as also shown in Fig. 3a and 3c (red dots), with a difference of approximately 5. Additionally, in May (at the onset of desalinization), the model slightly overestimates the observations, with a difference of approximately 2 (see also magenta dots in Fig. 3a,c).

The disparities observed between the modeled and observed salinity fields might result from differences in the time periods of data acquisition between the observations and the model, particularly considering the significant salinity variability near the channel occurring at a semi-diurnal scale. Additionally, uncertainties in the model drivers, especially concerning river discharge, could contribute to these discrepancies. Moreover, the relatively smooth bathymetry within the model may influence salinity outcomes; a shallower bathymetry could restrict salt intrusion into the lagoon during the salinization phase. Despite these considerations, the model demonstrates highly satisfactory statistical performance. The Nash-Sutcliffe efficiency coefficient (Nash &

Sutcliffe, 1970), the ratio of standard deviations, and root-mean-square error, for the surface (bottom, respectively) salinity of both the model and observations in the monthly mean are 0.96 (0.91), 0.92 (0.93), and 1.70 (2.64), respectively.

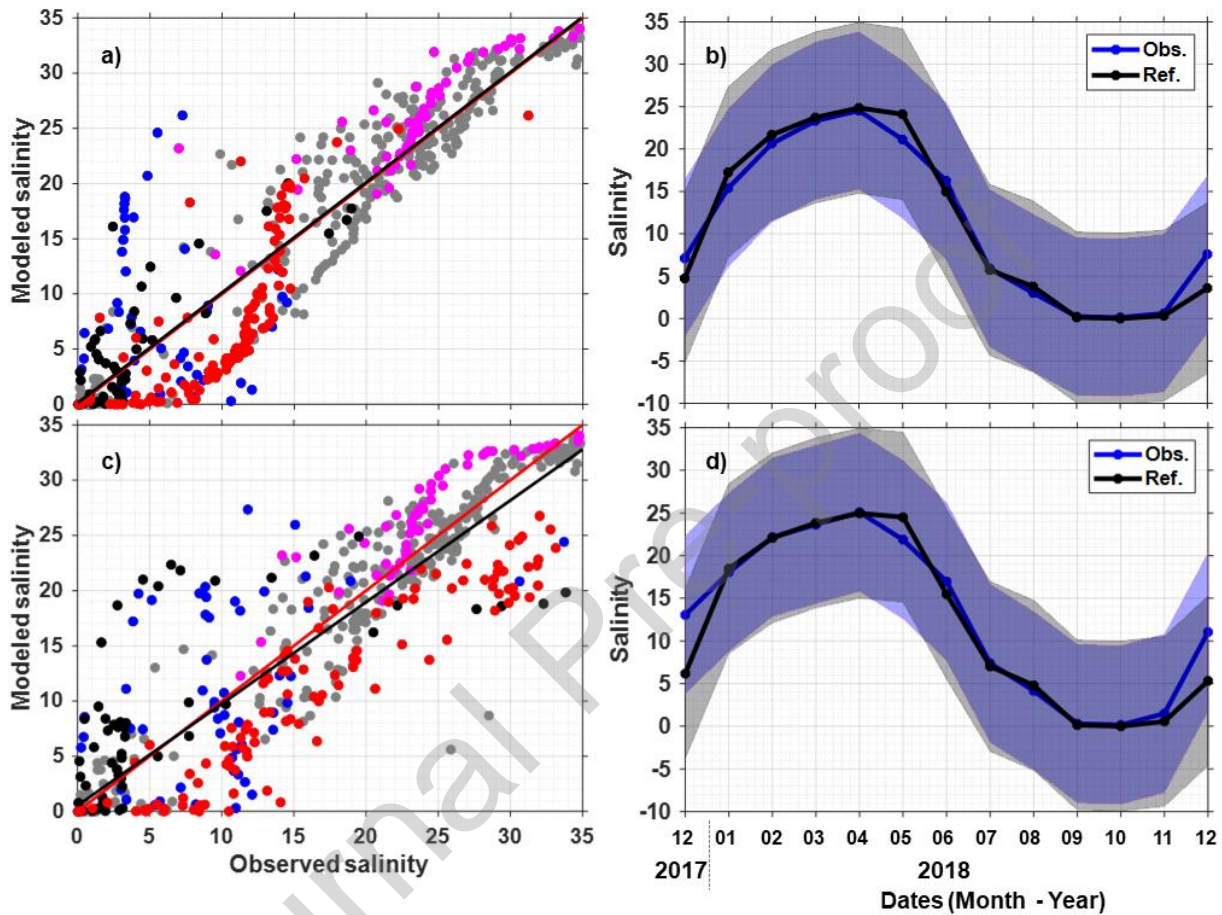


Fig. 3. Comparison of modeled and observed salinity fields. a, c) Scatter plots of modelled vs observed surface (a) and bottom (c) salinity at the CTD stations for the 13 field campaigns conducted from December 2017 to December 2018. The black line represents the linear relationship, while the red line depicts the 1:1 relationship. The magenta, blue, black, and red dots correspond to the months of May, July, August, and December, respectively, while the grey dots represent the rest of the year. b, d) Monthly mean surface salinity (d) and bottom salinity (b) between December 2017 and December 2018. The color shading indicates the range of ± 1 standard deviation around the monthly mean.

3.1.2. Lagoon stratification

Figure 4 shows the observed and modeled vertical structure of salinity along the high-resolution section between the entrance of Cotonou channel (South) and Sô river mouth (North) (white dashed line in Fig. 1c). In December 2017 and 2018, the southern lagoon's observed bottom salinity reaches 30, with a salinity difference of about 15 between the bottom and the surface salinity, while the stratification remains weak near the river mouth. In August 2018, the bottom salinity of the lagoon has increased, but the salinity difference between bottom and surface remains important (~10), despite the lagoon being shallow. Apart from this limited area in the south, the rest of the lagoon is filled with fresh water.

The model accurately reproduces the observed salt-wedge at the beginning of the salinization (Fig. 4a and 4d) and desalinization periods (Fig. 4b and e), which suggests that the density difference between salty ocean water and fresh river water, along with associated gravity currents, may play a significant role in salt penetration in the lagoon (Okpeitcha et al., 2022). The presence of this fine-scale vertical salinity structure provides further confidence in the model's ability to reproduce the lagoon hydrodynamics and the dispersion of salt.

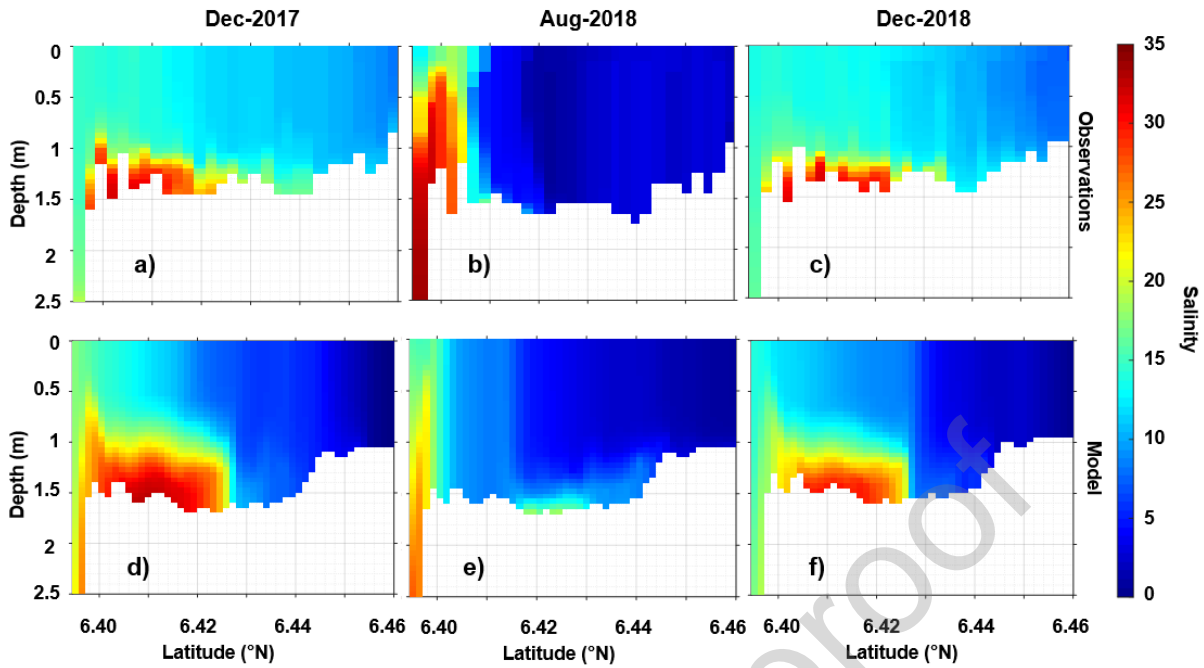


Fig. 4. Vertical salinity structure of the Nokoué Lagoon along a south-north section from the entrance of the Cotonou Channel (south) to the mouth of the Sô River (north) during the salinization (December) and desalination (August) phases. The upper panel shows observations, while the lower panel shows model results. The location of the south-north section can be found in Fig. 1.

3.1.3. Water-level variation

We present a comparison of the water level observed at a specific point located south of the Nokoué lagoon (marked by a red square in Fig. 1) with the corresponding model results. The model successfully simulates the different scales of water level variability observed by Chaigneau et al., (2022), including the seasonal variations and the 14-day cycle associated with spring and neap tides (Chaigneau et al., 2022; Morel et al, 2022) (Fig. 5a). However, the maximum water level during the peak of the wet season is underestimated by the model by ~5 cm compared to the observations. Additionally, the tidal amplitudes are slightly overestimated in the model (~6-7 cm) compared to the observations (~3-5 cm) at the location of the observation, but the model reproduces the tidal phase consistently with the observations. We note that the

peaks in the observations are related to a seiche phenomenon (Chaigneau et al., 2022) which are not represented in the model due to the absence of high-frequency winds and squall lines in the ECMWF fields used for atmospheric forcing.

Despite the discrepancies between observations and model results at high frequencies, the modelled water-level variations match the observed variations well (Fig. 5b). The Nash–Sutcliffe efficiency coefficient, ratio of standard deviation and root-mean-square error for both model and observations are 0.86, 0.94 and 0.08 m, respectively.

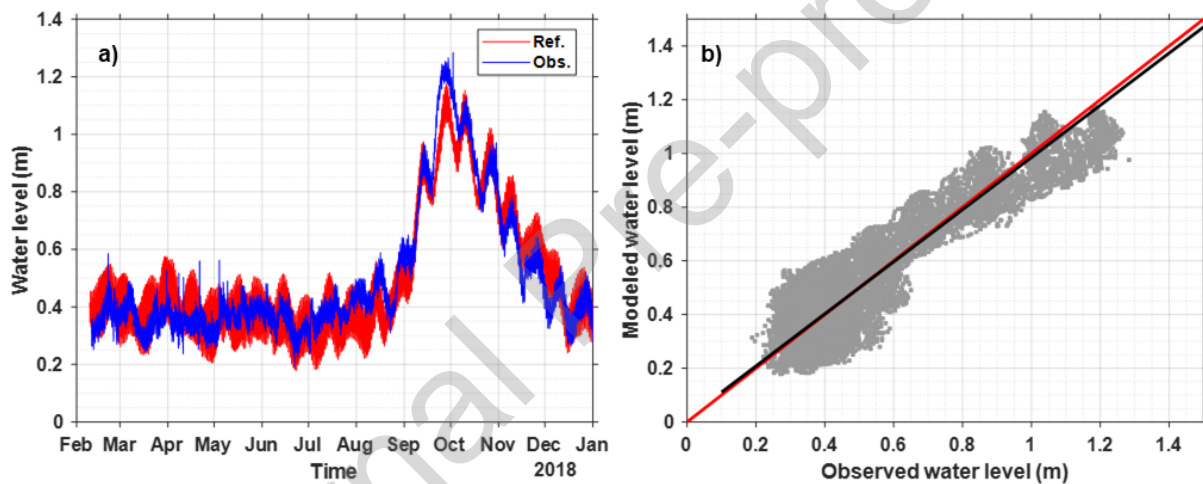


Fig. 5. Comparison of modelled and observed water-level time series from February 2017 to December 2018. a) Time series variation of water-level. b) Scatter plot showing the relationship between modeled and observed water-level datasets. The black line represents the linear relationship, while the red line depicts the 1:1 relationship.

In summary, the good qualitative and quantitative agreement between the simulated and observed salinity and water-level variations demonstrate that the model accurately reproduces the lagoon dynamics. Hence in the following, we use the various simulations to understand the physical processes and mechanisms driving the observed salinity variations in the lagoon. We note that the long and narrow Cotonou channel makes this lagoon a strongly choked system, and the differences in the

observed and modelled water-level variations at both high and low frequencies are consistent with a lack of dissipation in the channel, possibly related to the presence of large pylons of three bridges and rocky blocks obstructing the channel entrance, which are not considered in the current model configuration.

3.2. Main drivers of the Nokoué lagoon salinity

In this section, we aim to gain a deeper understanding of the individual contributions of the main forcings - tide, baroclinic fluxes related to salt gradients, winds, and freshwater fluxes - to the salinity dynamics of Nokoué lagoon. To do so, we analyze the results of the simulations, including the *NoTide*, *NoSal*, *NoWind*, and *RunOffs* scenarios. Note that in this analysis, results from surface and bottom level simulations are consistent, and therefore, we focus on the surface results only in the following discussion.

3.2.1. Global impact of the main forcings on seasonal salinity variations

Fig. 6 shows the daily mean surface salinity of the *Ref* simulation (red curve) from November 2017 to December 2018. From November to February, the salinity increases progressively from 0 to 22, marking the salinization phase. From mid-February to May, the salinity remains quasi-stable at around 22-25, representing the quasi-equilibrium phase. From May to October, the salinity decreases rapidly from 25 to 0, marking the desalination phase. We will focus on the salinization and desalination phases in the following analysis.

Global impact of specific forcings can be inferred from the simulations removing driving processes. This demonstrates the importance of the tide but also of the wind and the baroclinic effects in determining the global salinity level of the lagoon. The mean surface salinity in *NoTide* (blue curve) and *NoSal* (black curve) follows a similar

variability to the *Ref* simulation, but with significantly lower intensities. The salinity in *NoTide* varies from 0 to 10 from November to February, from 10 to 18 from February to May and 18 to 0 from May to October. In the *NoTide* and *NoSal* experiments, quasi-equilibrium is not reached, and the variation in salinity from February to May is much greater than in *Ref*. *NoSal* remains less salty than *NoTide* with a difference of ~ 2 in salinity between February and June, highlighting the crucial role of the baroclinic effect in the salinization mechanism of the lagoon.

In the *NoWind* simulation, the salinity is greater than in *Ref* but follows a similar variation. The difference in salinity between the *Ref* and *NoWind* simulations is ~ 5 . The impact of the wind forcing on the salinity dynamics will be further discussed in the following analysis.

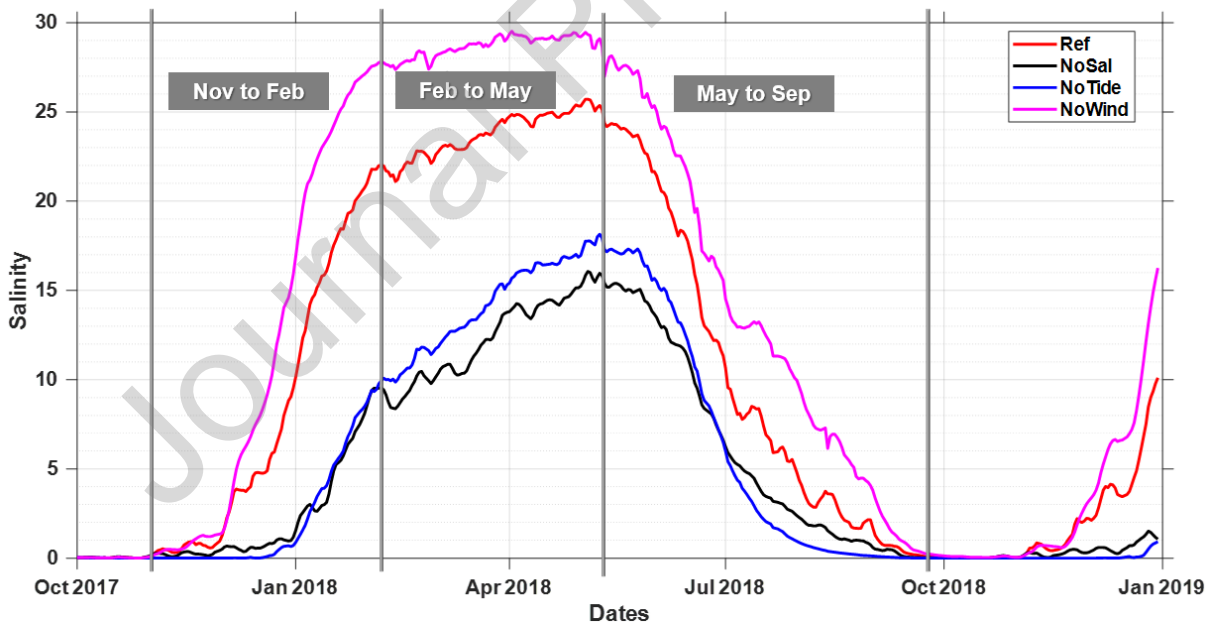


Fig. 6. Daily mean lagoon surface salinity variations for the *Ref* (red), *NoTide* (blue), *NoSal* (black) and *NoWind* (magenta) simulations, and selected phases.

3.2.2. Tidal, baroclinic and wind effects during the salinization phase

Here we aim to assess the total change in salinity during the salinization phase (November-February) for each simulation. To achieve this, as explained in Section 2.4, we analyze the total salt fluxes throughout the entire salinization phase, as well as the average fluxes at different temporal scales. However, we observed that fluxes at intermediate frequencies (24h50 to 15 days) are significantly weaker. Hence, we focus on high frequency (i.e., periods <24h50) and low frequency (i.e., periods >15 days) scales.

During the salinization phase (Fig. 7), the *Ref* simulation shows that the mean horizontal salt fluxes structure (Fig. 7e) is similar to that of the high-frequency fluxes (Fig. 7i), but the latter are more intense. The high intensity of salt flux at high frequency in the southern part of the lagoon (Fig. 7i) indicates the important role of the tide in supplying salt to this region. For the rest of the lagoon, high-frequency processes play important role in spreading the saltwater from the southern input to the entire lagoon. The low-frequency horizontal mean circulation (Fig. 7m), on the other hand, has the opposite effect and is mainly directed from the rivers towards the Cotonou Channel. This is due to the inflow of freshwater from the rivers, which tends to 'push back' some of the salt water from the river mouths, leading to weaker salinity variations in these regions during the salinization phase. Therefore, low frequency fluxes are related to freshwater inflows and reduce salinization by high frequency fluxes, related to tidal and other high-frequency processes.

In the *NoTide* simulation, salinity variations are significantly lower compared to the *Ref* simulation (Fig. 7b vs. Fig. 7a, also Fig. 6). Nevertheless, the spatial distribution of salinity in the two simulations shows strong similarities (Fig. 7a and b), with high values in the southeast and low values in the north. High-frequency processes drive

salinization in both *Ref* and *NoTide* simulations (Fig. 7f and j), while low-frequency fluxes (Fig. 7n) limit it. Similar to the *Ref* simulation, the *NoTide* simulation shows similarities at low-frequencies (Fig. 7m and n), confirming that tidal effects are not involved in low-frequency variability, which is mostly associated with river discharges. The major differences between the *Ref* and *NoTide* simulations are at high frequency, mostly at the channel mouth, where the flux intensity is significantly lower in the *NoTide* simulation (Fig. 7i and j). Thus, the *NoTide* simulation confirms that the tide plays a major role in the salt input to the south of the lagoon, which then spreads throughout the lagoon through other high-frequency processes limited by low-frequency fluxes generated by the rivers. Overall, this confirms that the tide is crucial for the overall salt input into the lagoon, but other processes such as baroclinic flows and winds also play an important role in the redistribution of southern salt input within the lagoon.

In the *NoSal* simulation, salt is a passive tracer inside the lagoon, and its influence on dynamics is eliminated (see Section 2.2.3). The mean flux (Fig. 7g) and high-frequency flux (Fig. 7k) are similar but very different from their counterparts in the *Ref* simulation (Fig. 7e and i). Baroclinic effects related to salt gradients increase salt supply at the mouth of the channel in the south of the lagoon, but mainly allow for its redistribution throughout the lagoon by high frequency processes. The low-frequency salt fluxes are again similar to *Ref* and *NoTide* simulations, confirming their association with inflow of fresh water from the rivers. Overall, without the effect of salt gradients and under tidal conditions, the lagoon becomes slightly less salty than in the *NoTide* experiment (see also Fig. 6). Only the southwestern region of the lagoon near the mouth is saltier than the *NoTide* experiment (Fig. 7c).

In the *NoWind* simulation, the mean fluxes are similar to *Ref*, except in the North-East of the lagoon, where the mean and high-frequency salt fluxes are much

stronger. The penetration of salt is associated with high-frequency fluxes, while low-frequency fluxes exhibit some differences. This is expected as a baroclinic circulation associated with the mean wind is anticipated, with water pushed in the direction of the wind at the surface and the opposite effect at the bottom (Bernardi et al., 2012; Cerralbo et al., 2016; Lacy et al., 2003; O’Callaghan & Stevens, 2011). However, the most striking effect is that high-frequency variability associated with the wind keeps the saltwater from penetrating further to the North-East.

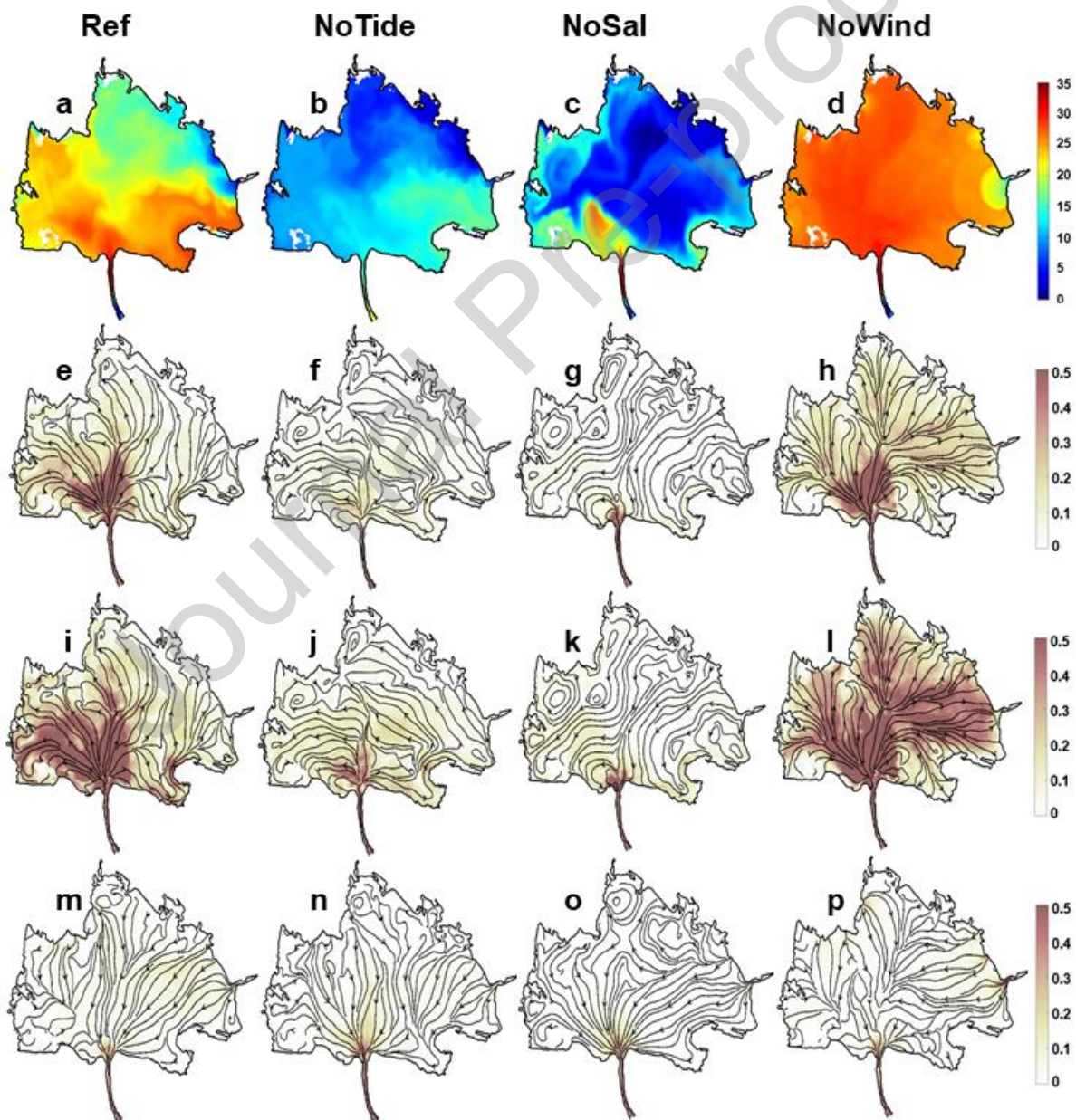


Fig. 7. Salinity and salt flux evolution during the salinization period (November to February). Upper panel: Total surface salinity variability (difference between February and November surface salinity) for a) Ref, b) NoTide, c) NoSal and d) NoWind simulations. Second panel from the top: Total mean salt flux. Third panel from the top: high-frequency (<24h50) salt flux. Lower panel: low-frequency (>15 days) salt flux. The salt flux unit is PSU m s⁻¹, and streamlines represent the direction of the salt flux propagation.

To analyse this effect, an additional simulation (not shown here) was conducted with seasonal (low frequency) wind forcing. This simulation resulted in a salinity structure and fluxes that were very close to the *Ref* simulation, showing that the high-frequency variations of the wind itself plays no role in limiting the salt penetration to the North-East. Our interpretation of this counterintuitive result is that the permanent winds generate small scale and high-frequency circulations, either through shear instabilities or under the influence of topography. Indeed, as shown by Fig. 8, daily outputs of the current and salinity fields confirm the generation of horizontal recirculation patterns at small-scale and high-frequency when the wind is taken into account and that these features disappear in the *NoWind* configuration. The instantaneous (daily) salinity distribution in the lagoon is also strongly correlated with the streamlines, in particular at small scales, showing the influence of eddies in the redistribution of salt. Further studies are required to confirm this interpretation and analyse the details of the processes responsible for the generation of these small-scale recirculation patterns.

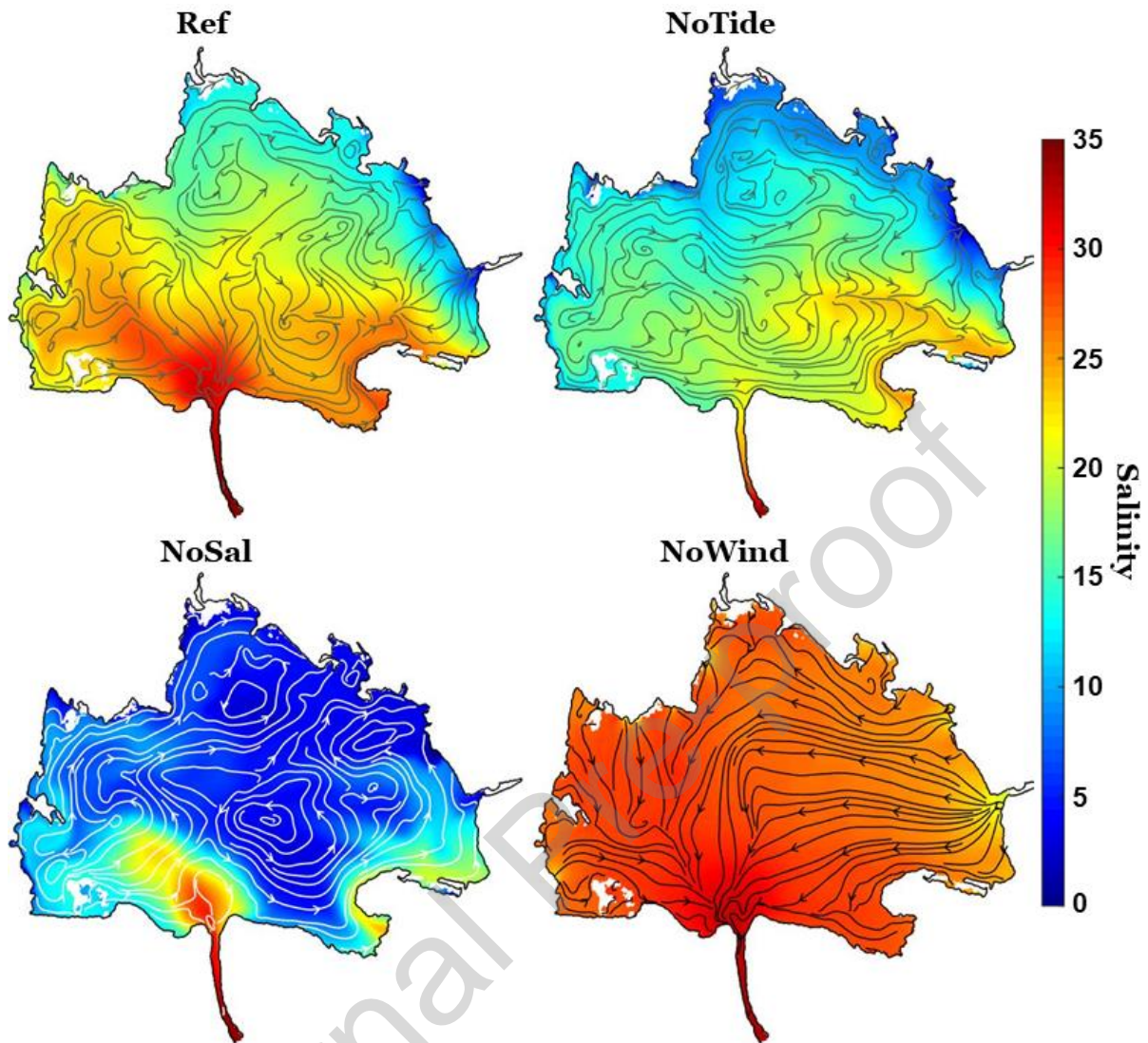


Fig. 8. Instantaneous surface salinity and current streamlines on the 27th of February during the salinization phase for Ref, NoTide, NoSal and NoWind simulations. Note the strong correlation between salinity distribution and small scale circulation patterns.

To conclude, the experiments conducted reveal that tide-driven high-frequency fluxes transport a significant amount of salt from the ocean to the southern part of the lagoon through the Cotonou channel. Although the initial salt input at the mouth of the lagoon is critical, other processes are involved in the salinization of the entire lagoon. The high frequency baroclinic fluxes intensify the salinity input at the south and promote the redistribution of salt by gravity throughout the lagoon. Despite its

shallowness, the pressure gradient associated with the salt plays important role in the penetration of saltwater in the lagoon. The rivers supply a permanent flow of fresh water that limits the salinization of the entire lagoon. Lastly, wind patterns alter the low-frequency fluxes but their primary effect is to generate small-scale and high-frequency currents, that partially inhibit the salinization of the north-eastern part of the lagoon.

3.2.3. River discharge effects

In this section we investigate the impact of river inflow rates on the equilibrium salinity structure in the lagoon and the threshold at which complete desalinization can be achieved. Figure 9a shows an overview of the monthly salinity evolution in 6 of the 13 *RunOffs* simulations, all starting with a same condition from May 1, 2018, of the *Ref* simulation. As expected, the more intense the river inflow, the faster the lagoon desalinizes. There is a clear salt gradient between the north-east and south-west of the lagoon, with the southern part remaining saltier due to the presence of brackish water near the mouth of the Cotonou channel, which gradually disappears as the flow increases. However, desalinization in most parts of the lagoon occurs much more rapidly.

Figure 9b summarizes the results of the 13 scenarios and shows the average value of the final surface salinity attained by the lagoon at equilibrium as a function of the prescribed total river discharge (blue curve). At the end of the dry season (May), the river flux in the *Ref* experiment is $7.5 \text{ m}^3 \text{ s}^{-1}$, and the mean value of the surface salinity is about 25 (see Fig. 3). This final average salinity decreases rapidly with higher river fluxes, varying from 13 for river flows of $30 \text{ m}^3 \text{ s}^{-1}$ to 7 for flows of $90 \text{ m}^3 \text{ s}^{-1}$, which is consistent with the findings of Okpeitcha et al (2022) using a simplified box model. The present experiment confirms this (Fig. 9b -blue curve-) by demonstrating that increasing the river discharge by $\sim 15 \text{ m}^3 \text{ s}^{-1}$ is required to decrease the average

salinity from 25 to 16. Above $100 \text{ m}^3 \text{ s}^{-1}$, the final average salinity in the lagoon falls below ~ 5 and varies less rapidly due to the maintenance of a salinity bulge at the lagoon entrance associated with the tide. When the flow rate reaches $500 \text{ m}^3 \text{ s}^{-1}$ and above, the entire lagoon becomes desalinated. It is also apparent from Fig. 9a that regardless of the river flux value, the salinity of the lagoon reaches a state of equilibrium after a certain time interval. The red curve in figure 9b shows the time taken for the lagoon's salinity to reach this equilibrium, which decreases as the river flow increases, ranging from 30 to 9 days for flows between 30 and $280 \text{ m}^3 \text{ s}^{-1}$. For flow values above $280 \text{ m}^3 \text{ s}^{-1}$, this time is almost constant at ~ 5 days.

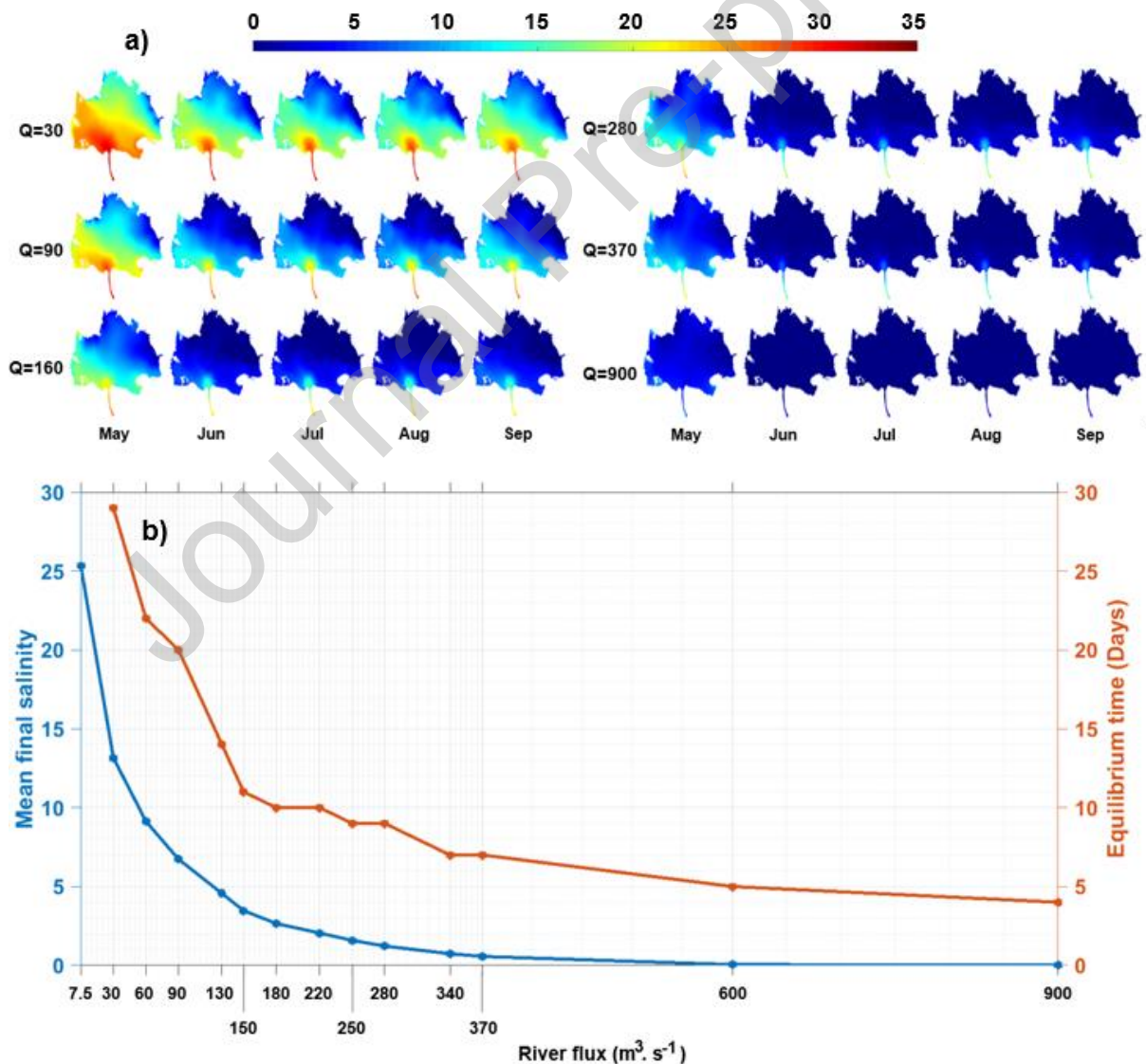


Fig. 9. a) Spatiotemporal surface salinity variability in response to river fluxes (Q , in $m^3 s^{-1}$). b) Relationship between final mean surface salinity (blue curve) and time required to reach equilibrium (red curve) of the lagoon under different river flows.

4. Conclusion

We developed a 3D numerical configuration, based on the SYMPHONIE model, to study the salinity variations of the Nokoué lagoon. The model accurately reproduced various features of the observed salinity and water level of the lagoon. To study the processes responsible for salt dispersion in the lagoon, we performed sensitivity studies by removing key drivers (tide, wind, influence of salinity on density) or modifying rivers inflow.

We first analyzed the evolution of the mean lagoon salinity for three experiments: *NoTide*, *NoSal*, and *NoWind*. Although these experiments showed a similar pattern to the reference simulation, the intensities were significantly different. The maximum average salinity reached in April in the reference simulation was 25, whereas in *NoTide* and *NoSal*, it was only 17 and 15, respectively, and was reached in May. This result highlights the strong influence of the tide in salt penetration into the lagoon but also underlines the important role played by the baroclinic effect despite the lagoon's shallowness. In the *NoWind* simulation, the salinity was ~ 5 greater than in reference simulation.

Our analysis of the role of tide, salt gradient and wind on the lagoon salinization revealed that high-frequency fluxes associated with the ocean tide import a significant amount of salt from the ocean via the Cotonou channel to the South of the lagoon, and that this initial salt input is crucial for the salinization of the rest of the lagoon. High-frequency baroclinic fluxes increase this initial local input of salt in the South and

redistribute salt throughout the whole lagoon via gravity and baroclinic pressure gradients. Finally, low-frequency winds generate high-frequency recirculation that partially prevent the salinization of the North-East of the lagoon.

The rivers provide a permanent flux of fresh water, which limits the salinization of the lagoon. The equilibrium salinity of the lagoon decreases with increasing river flux and reaches a steady state within 2 months of the simulations' start, with the presence of a layer of brackish water in the southwestern part of the lagoon. Above $100 \text{ m}^3 \text{ s}^{-1}$, the final average salinity remains below 5, and above $500 \text{ m}^3 \text{ s}^{-1}$, the entire lagoon is desalinated. At low flow conditions (equivalent to average salinity above 5) Nokoué lagoon is highly sensitive to even small changes in river discharge.

The model developed is a valuable tool for managing the lagoon, such as evaluating the impact of a dam construction, which regulates flows entering the lagoon, on the lagoon salinity and therefore on its ecosystem. The study improves our understanding of the Nokoué lagoon salinity dynamics and West African coastal lagoons more generally.

Future research on the Nokoué lagoon should account for the three bridges crossing the Cotonou channel and the rocky blocks to more accurately represent the dissipation that influences the salinity initial input in the south of the lagoon and its distribution within the lagoon. Additional studies are also needed to investigate further the development of high-frequency recirculation patterns associated with the permanent wind, which may be related to bathymetry gradients or shear instabilities of the mean currents.

Acknowledgements

Field surveys and instrumentation were supported by IRD, with contributions from ANR @RAction chair medLOC (ANR-14-ACHN-0007-01–T. Stieglitz). V. Okpeitcha was funded by OmiDelta project of the Embassy of the Kingdom of the Netherlands in Benin, through a scholarship grant of the National Institute of Water (INE/UAC). This work is a contribution to the « JEA1 SAFUME » project funded by IRD. Special thanks to the members and crew participating to the monthly surveys, and in particular A. Assogba, M. Benoist, and J. Azankpo. Collaboration of Team 2/ODA-INE is also acknowledged. This work is also part of the "Lagune Nokoué" TOSCA project funded by the French National Center for Space Studies (CNES). This work was granted access to the HPC resources of CALMIP supercomputing center under the allocation p18033.

References

- Abimbola, O. P., Mittelstet, A. R., Messer, T. L., Berry, E. D., Bartelt-hunt, S. L., & Hansen, S. P. (2020). Science of the Total Environment Predicting Escherichia coli loads in cascading dams with machine learning: An integration of hydrometeorology, animal density and grazing pattern. *Science of the Total Environment*, 722, 137894. <https://doi.org/10.1016/j.scitotenv.2020.137894>
- Ahokossi, Y. (2018). Analysis of the rainfall variability and change in the Republic of Benin (West Africa). *Hydrological Sciences Journal*, 63(15–16), 2097–2123. <https://doi.org/10.1080/02626667.2018.1554286>
- Alekseenko, E., Roux, B., Fougere, D., & Chen, P. G. (2017). The effect of wind induced bottom shear stress and salinity on *Zostera noltii* replanting in a Mediterranean coastal lagoon. *Estuarine, Coastal and Shelf Science*, 187, 293–305.
- Aluie, H., Hecht, M., & Vallis, G. K. (2018). Mapping the energy cascade in the North Atlantic Ocean: The coarse-graining approach. *Journal of Physical Oceanography*, 48(2), 225–244.
- Arakawa, A., & Lamb, V. R. (1977). Computational design of the basic dynamical processes of the UCLA general circulation model. *General Circulation Models of the Atmosphere*, 17(Supplement C), 173–265.
- Attrill, M. J. (2002). A testable linear model for diversity trends in estuaries. *Journal of Animal Ecology*, 71(2), 262–269. <https://doi.org/10.1046/j.1365-2656.2002.00593.x>
- Auclair, F., Marsaleix, P., & Estournel, C. (2000). Sigma coordinate pressure gradient errors: evaluation and reduction by an inverse method. *Journal of Atmospheric and Oceanic Technology*, 17(10), 1348–1367.

- Bajamngigni Gbambie, A. S., & Steyn, D. G. (2013). Sea breezes at Cotonou and their interaction with the West African monsoon. *International Journal of Climatology*, 33(13), 2889–2899. <https://doi.org/10.1002/joc.3637>
- Barnes, R. S. K. (1980). *Coastal lagoons* (Vol. 1). CUP Archive.
- Bernardi, D., Caleffi, V., Gasperini, L., Schippa, L., & Valiani, A. A. (2012). Study of the Hydrodynamics of the Coastal Lagoon “Valli di Comacchio.” *Proceedings of the 3rd International Symposium on Shallow Flows, Iowa City, IA, USA*, 4–6.
- Biao, E. I. (2017). Assessing the impacts of climate change on river discharge dynamics in Oueme River basin (Benin, West Africa). *Hydrology*, 4(4). <https://doi.org/10.3390/hydrology4040047>
- Blumberg, A. F., & Mellor, G. L. (1987). A description of a three-dimensional coastal ocean circulation model. *Three-dimensional coastal ocean models*, 4, 1-16. <https://doi.org/10.1029/CO004p0001>
- Bretherton, F. P., Davis, R. E., & Fandry, C. B. (1976). A technique for objective analysis and design of oceanographic experiments applied to MODE-73. *Deep-Sea Research and Oceanographic Abstracts*, 23(7), 559–582. [https://doi.org/10.1016/0011-7471\(76\)90001-2](https://doi.org/10.1016/0011-7471(76)90001-2)
- Carrere, L., Lyard, F., Cancet, M., Guillot, A., & Picot, N. (2016). *FES2014, a new tidal model–Validation results and perspectives for improvements, presentation to ESA Living Planet Conference*. Prague.
- Cerralbo, P., Espino, M., & Grifoll, M. (2016). Modeling circulation patterns induced by spatial cross-shore wind variability in a small-size coastal embayment. *Ocean Modelling*, 104, 84–98. <https://doi.org/10.1016/j.ocemod.2016.05.011>
- Chaigneau, A., Okpeitcha, O. V., Morel, Y., Stieglitz, T., Assogba, A., Benoist, M., Allamel, P., Honfo, J., Awoulmbang Sakpak, T. D., Rétif, F., Duhaut, T., Peugeot,

- C., & Sohou, Z. (2022). From seasonal flood pulse to seiche: Multi-frequency water-level fluctuations in a large shallow tropical lagoon (Nokoué Lagoon, Benin). *Estuarine, Coastal and Shelf Science*, 267. <https://doi.org/10.1016/j.ecss.2022.107767>
- Chaigneau, A., Ouinsou, F. T., Akodogbo, H. H., Dobigny, G., Avocegan, T. T., Dossou-Sognon, F. U., Okpeitcha, V. O., Djihouessi, M. B., & Azémar, F. (2023). Physicochemical Drivers of Zooplankton Seasonal Variability in a West African Lagoon (Nokoué Lagoon, Benin). *Journal of Marine Science and Engineering*, 11(3), 556. <https://doi.org/10.3390/jmse11030556>
- Costa, A., Doglioli, A. M., Marsaleix, P., & Petrenko, A. A. (2017). Comparison of in situ microstructure measurements to different turbulence closure schemes in a 3-D numerical ocean circulation model. *Ocean Modelling*, 120, 1-17. <https://doi.org/10.1016/j.ocemod.2017.10.002>
- Cromwell, J. E. (1971). Barrier coast distribution: a world-wide survey. *Abstracts, Second Coastal and Shallow Water Research Conference, US Office of Naval Research Geography Program, University Press, University of Southern California, Los Angeles, California.*
- Damien, P. (2015). *Etude de la circulation océanique en Méditerranée Nord-Occidentale à l'aide d'un modèle numérique à haute résolution: influence de la submésoséchelle* [Université Toulouse III Paul Sabatier]. <http://thesesups.ups-tlse.fr/2682/1/2015TOU30024.pdf>
- Djihouessi, M. B., & Aina, M. P. (2018). A review of hydrodynamics and water quality of Lake Nokoué: Current state of knowledge and prospects for further research. *Regional Studies in Marine Science*, 18, 57–67. <https://doi.org/10.1016/j.rsma.2018.01.002>

- Djihouessi, M. B., Aina, M. P., Kpanou, B.-V., & Kpondjo, N. (2017). Measuring the Total Economic Value of Traditional Sand Dredging in the Coastal Lagoon Complex of Grand-Nokoué (Benin). *Journal of Environmental Protection*, 08(13), 1605–1621. <https://doi.org/10.4236/jep.2017.813099>
- Djihouessi, M. B., Djihouessi, M. B., & Aina, M. P. (2019). A review of habitat and biodiversity research in Lake Nokoué, Benin Republic: Current state of knowledge and prospects for further research. *Ecohydrology & Hydrobiology*, 19(1), 131–145.
- Dube, A., Jayaraman, G., & Rani, R. (2010). Modelling the effects of variable salinity on the temporal distribution of plankton in shallow coastal lagoons. *Journal of Hydro-Environment Research*, 4(3), 199–209. <https://doi.org/10.1016/j.jher.2010.03.003>
- Fairall, C. W., Bradley, E. F., Hare, J. E., Grachev, A. A., & Edson, J. B. (2003). Bulk parameterization of air–sea fluxes: Updates and verification for the COARE algorithm. *Journal of climate*, 16(4), 571-591. [https://doi.org/10.1175/1520-0442\(2003\)016<0571:BPOASF>2.0.CO;2](https://doi.org/10.1175/1520-0442(2003)016<0571:BPOASF>2.0.CO;2)
- Fink, A. H., Engel, T., Ermert, V., van der Linden, R., Schneidewind, M., Redl, R., Afiesimama, E., Thiaw, W. M., Yorke, C., & Evans, M. (2017). Mean climate and seasonal cycle. In D. J. Parker & M. Diop-Kane (Eds.), *Meteorology of tropical West Africa: The forecasters' handbook* (pp. 1–39). Wiley Online Library.
- Franco, T. P., Neves, L. M., & Araújo, F. G. (2019). Better with more or less salt? The association of fish assemblages in coastal lagoons with different salinity ranges. *Hydrobiologia*, 828, 83–100.
- Gadel, F., & Texier, H. (1986). Distribution and nature of organic matter in recent sediments of Lake Nokoué, Benin (West Africa). *Estuarine, Coastal and Shelf Science*, 22(6), 767–784. [https://doi.org/10.1016/0272-7714\(86\)90098-3](https://doi.org/10.1016/0272-7714(86)90098-3)

- García-Oliva, M., Marcos, C., Umgieser, G., McKiver, W., Ghezze, M., De Pascalis, F., & Pérez-Ruzafa, A. (2019). Modelling the impact of dredging inlets on the salinity and temperature regimes in coastal lagoons. *Ocean and Coastal Management*, 180(August), 104913. <https://doi.org/10.1016/j.ocecoaman.2019.104913>
- Gnohossou, P. (2006). *La faune benthique d'une lagune ouest Africaine (le lac Nokoue au Bénin), diversité, abondance, variations temporelles et spatiales, place dans la chaîne trophique* [Université de Toulouse > Institut National Polytechnique de Toulouse - Toulouse INP (FRANCE)]. <http://ethesis.inp-toulouse.fr/archive/00000481/>
- Gonenc, I. E., & Wolflin, J. P. (2004). *Coastal lagoons: ecosystem processes and modeling for sustainable use and development*. CRC Press.
- Gross, E. S., Koseff, J. R., & Monismith, S. G. (1999). Three-dimensional salinity simulations of south San Francisco Bay. *Journal of Hydraulic Engineering*, 125(11), 1199–1209.
- Guedje, F. K., Houeto, A. V. V., Houngrinou, E. B., Fink, A. H., & Knippertz, P. (2019). Climatology of coastal wind regimes in Benin. *Meteorologische Zeitschrift*, 28(1), 23–39. <https://doi.org/10.1127/metz/2019/0930>
- Guragai, B., Hashimoto, T., Oguma, K., & Takizawa, S. (2018). Data logger-based measurement of household water consumption and micro-component analysis of an intermittent water supply system. *Journal of Cleaner Production*, 197, 1159–1168. <https://doi.org/10.1016/j.jclepro.2018.06.198>
- Kjerfve, B. (1994). Coastal lagoons. In *Elsevier oceanography series* (Vol. 60, pp. 1–8). Elsevier.
- Lacy, J. R., Stacey, M. T., Burau, J. R., & Monismith, S. G. (2003). Interaction of lateral

- baroclinic forcing and turbulence in an estuary. *Journal of Geophysical Research: Oceans*, 108(3), 1–15. <https://doi.org/10.1029/2002jc001392>
- Lalèyè, A. P., Villanueva, M. C., Entsua, M. M., & Moreau, J. (2007). A review of the aquatic living resources in Gulf of Guinea lagoons, with particular emphasis on fisheries management issues. *Journal of Afrotropical Zoology*, 3(Special issue), 123–136.
- Laleye, P. (1995). Ecologie comparée de deux espèces de Chrysichthys, poissons siluri-formes (Claroteidae) du complexe lagunaire lac Nokoué-lagune de Porto-Novo au Bénin. In *Tropicultura* (Vol. 13, Issue 4). Univ. Liège (Belgique).
- Lalèyè, P., Niyonkuru, C., Moreau, J., & Teugels, G. G. (2003). Spatial and seasonal distribution of the ichthyofauna of lake nokoué, bénin, west africa. *African Journal of Aquatic Science*, 28(2), 151–161. <https://doi.org/10.2989/16085910309503779>
- Latifou, A. B., Toko, I. I., Elegbe, H. A., Pelebe, R. O. E., Tougan, P. U., Boni, A. R., Ahyi, V., Hossou, E. S., VISSIENNON, Z., & Chikou, A. (2020). *Les Produits Halieutiques au Bénin: Sources d'Approvisionnement et Statistiques [Halieutic Products in BENIN: Supply Source and Statistics]*.
- Lawin, A. E., Houngouè, R., M'Po, Y. N. T., Houngouè, N. R., Attogouinon, A., & Afouda, A. A. (2019). Mid-century climate change impacts on Ouémé River discharge at Bonou Outlet (Benin). *Hydrology*, 6(3). <https://doi.org/10.3390/hydrology6030072>
- Le Barbé, L., Alé, G., Texier, H., Borel, Y., & Gualde, R. (1993). Les ressources en eaux superficielles de la République du Bénin. In *MONOGRAPHIES HYDROLOGIQUES* (ORSTOM). Institut Français de Recherche Scientifique pour le Développement en Coopération. http://horizon.documentation.ird.fr/exl-doc/pleins_textes/divers08-01/39537.pdf
- Lellouche, J.-M., Le Galloudec, O., Drévilion, M., Régnier, C., Greiner, E., Garric, G.,

- Ferry, N., Desportes, C., Testut, C.-E., & Bricaud, C. (2013). Evaluation of global monitoring and forecasting systems at Mercator Océan. *Ocean Science*, 9(1), 57–81.
- Mahanty, M. M., Mohanty, P. K., Pattnaik, A. K., Panda, U. S., Pradhan, S., & Samal, R. N. (2016). Hydrodynamics, temperature/salinity variability and residence time in the Chilika lagoon during dry and wet period: Measurement and modeling. *Continental Shelf Research*, 125, 28–43.
- Mama, D. (2010). Méthodologie et résultats du diagnostic de l'eutrophisation du lac Nokoué (Bénin). In *Thèse*. Université de Limoges.
- Marsaleix, P., Auclair, F., & Estournel, C. (2006). Considerations on open boundary conditions for regional and coastal ocean models. *Journal of Atmospheric and Oceanic Technology*, 23(11), 1604-1613. <http://dx.doi.org/10.1175/JTECH1930.1>
- Marsaleix, P., Auclair, F., Duhaut, T., Estournel, C., Nguyen, C., & Ulses, C. (2012). Alternatives to the Robert–Asselin filter. *Ocean Modelling*, 41, 53–66.
- Marsaleix, P., Auclair, F., Floor, J. W., Herrmann, M. J., Estournel, C., Pairaud, I., & Ulses, C. (2008). Energy conservation issues in sigma-coordinate free-surface ocean models. *Ocean Modelling*, 20(1), 61–89. <https://doi.org/10.1016/j.ocemod.2007.07.005>
- Marsaleix, P., Michaud, H., & Estournel, C. (2019). 3D phase-resolved wave modelling with a non-hydrostatic ocean circulation model. *Ocean Modelling*, 136, 28-50. <https://doi.org/10.1016/j.ocemod.2019.02.002>
- McIntosh, P. C. (1990). Oceanographic data interpolation: Objective analysis and splines. *Journal of Geophysical Research*, 95(C8), 13529. <https://doi.org/10.1029/jc095ic08p13529>
- Morel, Y., Chaigneau, A., Olaègbè, V., & Stieglitz, T. (2022). Terrestrial or oceanic

- forcing ? Water level variations in coastal lagoons constrained by river inflow and ocean tides. *Advances in Water Resources*, 169(January), 104309. <https://doi.org/10.1016/j.advwatres.2022.104309>
- Nash, J. E., & Sutcliffe, J. V. (1970). River flow forecasting through conceptual models part I—A discussion of principles. *Journal of hydrology*, 10(3), 282-290.
- N'Tcha M'Po, Y., Lawin, E., Yao, B., Oyerinde, G., Attogouinon, A., & Afouda, A. (2017). Decreasing Past and Mid-Century Rainfall Indices over the Ouémé River Basin, Benin (West Africa). *Climate*, 5(3), 74. <https://doi.org/10.3390/cli5030074>
- Nunes, A., Larson, M., Fragoso, C. R., & Hanson, H. (2021). Modeling the salinity dynamics of a choked coastal lagoon and its impact on the Sururu mussel (*Mytella falcata*) population. *Regional Studies in Marine Science*, 45, 101807. <https://doi.org/10.1016/j.rsma.2021.101807>
- O'Callaghan, J., & Stevens, C. (2011). 2.09 - *Wind Stresses on Estuaries* (E. Wolanski & D. B. T.-T. on E. and C. S. McLusky (eds.); pp. 151–169). Academic Press. <https://doi.org/https://doi.org/10.1016/B978-0-12-374711-2.00211-4>
- Odountan, O. H., de Bisthoven, L. J., Koudenoukpo, C. Z., & Abou, Y. (2019). Spatio-temporal variation of environmental variables and aquatic macroinvertebrate assemblages in Lake Nokoué, a RAMSAR site of Benin. *African Journal of Aquatic Science*, 44(3), 219–231. <https://doi.org/10.2989/16085914.2019.1629272>
- Okpeitcha, O. V., Chaigneau, A., Morel, Y., Stieglitz, T., Pomalegni, Y., Sohoun, Z., & Mama, D. (2022). Seasonal and interannual variability of salinity in a large West-African lagoon (Nokoué Lagoon, Benin). *Estuarine, Coastal and Shelf Science*, 264. <https://doi.org/10.1016/j.ecss.2021.107689>
- Pairaud, I. L., Auclair, F., Marsaleix, P., Lyard, F., & Pichon, A. (2010). Dynamics of the semi-diurnal and quarter-diurnal internal tides in the Bay of Biscay. Part 2:

- Baroclinic tides. *Continental Shelf Research*, 30(3-4), 253-269.
<https://doi.org/10.1016/j.csr.2008.03.004>
- Pauly, D. (1975). On the ecology of a small West African lagoon. *Sonderdruck Aus Bd*, 24(1), 46–62.
- Texier, H., Colleuil, B., Profizi, J. P., & Dossou, C. (1980). Le lac Nokoué, environnement du domaine margino-littoral sud-béninois: bathymétrie, lithofaciès, salinité, mollusque et peuplements végétaux. *Bull. Inst. Géol. Bass. Aguit.. Bordeaux, N° 28*, 115–142.
- Toublanc, F., Ayoub, N. K., Lyard, F., Marsaleix, P., & Allain, D. J. (2018). Tidal downscaling from the open ocean to the coast: a new approach applied to the Bay of Biscay. *Ocean Modelling*, 124, 16-32.
<https://doi.org/10.1016/j.ocemod.2018.02.001>
- Wong, A. P. S., Johnson, G. C., & Owens, W. B. (2003). Delayed-mode calibration of autonomous CTD profiling float salinity data by χ -S climatology. *Journal of Atmospheric and Oceanic Technology*, 20(2), 308–318.
[https://doi.org/10.1175/1520-0426\(2003\)020<0308:DMCOAC>2.0.CO;2](https://doi.org/10.1175/1520-0426(2003)020<0308:DMCOAC>2.0.CO;2)
- Yehouenou, E. A. P., Adamou, R., Azehoun, P. J., Eдорh, P. A., & Ahoyo, T. (2013). Monitoring of heavy metals in the complex “Nokoué lake - Cotonou and Porto-Novo lagoon” ecosystem during three years in the Republic of Benin. *Research Journal of Chemical Sciences*, 3(5), 12–18.
https://www.researchgate.net/publication/255982357_Monitoring_of_Heavy_Metals_in_the_complex_Nokoue_lake_-Cotonou_and_Porto-Novo_lagoon_ecosystem_during_three_years_in_the_Republic_of_Benin%0Ahttp://search.ebscohost.com/login.aspx?direct=true&db=lah&AN=20
- Zandagba, J., Moussa, M., Obada, E., & Afouda, A. (2016). Hydrodynamic modeling

of Nokoué Lake in Benin. *Hydrology*, 3(4), 44.

<https://doi.org/10.3390/hydrology3040044>

CRedit authorship contribution statement

V.O. Okpeitcha: Conceptualization; Data curation; Formal analysis; Investigation; Methodology; Software; Writing - original draft; Writing - review & editing. **A. Chaigneau:** Conceptualization; Data curation; Investigation; Methodology; Software; Resources; Supervision; Funding acquisition; Writing - original draft; Writing - review & editing. **Y. Morel:** Investigation; Methodology; Software; Writing - original draft; Funding acquisition; Writing - review & editing. **T. Duhaut:** Model conceptualization; Numerical simulations; result analysis; review. **P. Marsaleix:** Numerical modeling; result analysis; review & editing. **F. Rétif:** Model conceptualization. **J. Honfo:** Results analysis. **T. Stieglitz:** Investigation; Funding acquisition; Writing - review & editing. **Z. Sohoun:** Resources. **L.O. Sintondji:** Project administration; Results analysis. **D. Mama:** Resources; Project administration; Supervision.

Declaration of interests

The authors declare that they have no known competing financial interests or personal relationships that could have appeared to influence the work reported in this paper.

The authors declare the following financial interests/personal relationships which may be considered as potential competing interests:

Highlights

- The Nokoué Lagoon's dynamics is accurately captured by the 3D SYMPHONIE model.
- High-frequency salt fluxes related to tides import salt to the South of the Lagoon.
- Baroclinic fluxes greatly contribute to the dispersion of salt across the Lagoon.

- Winds mitigate the salinization process in the North-Eastern part of the Lagoon.
- Nokoué Lagoon is highly sensitive to river discharge, especially during low flow.

Journal Pre-proof